RSC Advances

ROYAL SOCIETY OF CHEMISTRY

www.rsc.org/advances

Journal Name

ARTICLE

Large-scale growth of sharp gold nano-cones for single-molecule SERS detection†

Received 00th January 20xx,
Accepted 00th January 20xx

DOI: 10.1039/x0xx00000x

www.rsc.org/

Ling Zhang,[a, b, ‡] Hongwen Liu,[b, ‡] Luyang Chen,[b] Pengfei Guan,[b] Bin Chen,[c] Takeshi Fujita,[b] Yoshinori Yamaguchi,[d, e] Hiroshi Iwasaki,[d, e] Qi-Kun Xue,[b,f] Mingwei Chen[b,c, g] *

We report a novel approach for large-scale gold nano-cone growth by utilizing the open nanopore channels of nanoporous gold films as both the template for nano-cone growing and the delivery nano-pipes of reduction gas. Quasi-periodic nan- cone arrays can uniformly sprout on the centimeter-sized free-standing nanoporous gold films. The sharp nano-cones giv- rise to ultrahigh surface enhanced Raman scattering for single molecule detection from the focused electromagnetic fields at the cone apexes. The large-scale nano-cone decorated nanoporous gold films may serve as a high-performance SERS substrate for wide-range applications in ultrasensitive instrumentation and molecule diagnostics.

Introduction

Surface-enhanced Raman scattering (SERS) is a powerful analytical technique for probing and identifying organic and biological molecules. [1-3] Ultra-high SERS enhancements from nano-sized "hot spots" open up exciting capability to pursue the analytical limit of spectroscopic methods for single molecule detection. Numerous experimental studies have been focusing on synthesizing high-performance, reproducible plasmonic nanostructures by optimizing the various contributions to the SERS enhancements. [4-11] The enhancement factors larger than 10^7 are usually achieved from closely spaced interacting particles [7, 8] and nanostructures with sharp tips, corners and edges [4, 9, 10] where local electromagnetic fields are dramatically augmented because of the resonant excitation of localized surface plasmon and the lightning rod effect of highly curved metal surfaces. [12] Various configurations for amplifying local electromagnetic fields have been reported recently, such as two-dimensional ordered arrays of nanoparticles by nanospherical lithography, [13] nanodiamond/nanostart structures [14] and bowtie antenna by electron beam lithography. [15] Since aligned metallic nano-tips as plasmonic nanoantennas have relatively uniform and reproducible as both the template of nano-tip growth and the delivery nano-pipes of reduction gas. The sharp nano-tips with an apex smaller than 5 nm, uniformly distributed on centimeter-sized NPG substrates, are capable for the single molecule SERS detection. SERS effects for potential single molecule detection, several methods have been developed to fabricate the nano-tip based SERS substrates, for examples, gold-shell nanopyramids fabricated using colloidal silica as template,[16] gold-covered silicon nano-tip arrays fabricated by chemical etching,[17] and gold needle arrays made by Ar^+ ion irradiation.[18] However, those substrates are limited either by complicated and expensive fabrication processes or by poor reproducibility. Moreover, all of them have not been reported to realize sufficient SERS enhancements for the single molecule detection. [19] In this study, we report a novel and facile approach for synthesizing large-scale aligned gold nano-cones (NC) by utilizing nanoporous gold (NPG) as both the template of nano-cone growth and the delivery nano-pipes of reduction gas. The sharp nano-cones with an apex smaller than 5 nm, uniformly distributed on centimeter-sized NPG substrates, are capable for the single molecule SERS detection.

Free-standing nanoporous gold films prepared by dealloying have bicontinuous nanoporosity in which open pore channels and gold ligaments are connected through the entire films.[20-22] Though NPG is an outstanding plasmonic substrate for surface enhanced spectroscopy and small nanopores yield high SERS enhancements, [20] the lack of sharp edges and corners along with inadequate electromagnetic coupling between gold ligaments leads to the technical difficulty to

[a] School of Optical-Electrical and Computer Engineering, University of Shanghai for Science and Technology, Shanghai 200093, P. R. China;
[b] WPI-Advanced Institute for Materials Research, Tohoku University, Sendai 980-8577, Japan; E-mail: mwchen@wpi-aimr.tohoku.ac.jp
[c] School of Materials Science and Engineering, Shanghai Jiao Tong University, Shanghai 200030, China
[d] PARC, Graduate School of Engineering, Osaka University, Osaka 565-0871, Japan
[e] Department of Applied Physics, Graduate School of Engineering, Osaka University, Osaka 565-0871, Japan
[f] Department of Physics, Tsinghua University, Beijing 100084, China
[g] CREST, Japan Science and Technology Agency (JST), Saitama 332-0012, Japan

† Electronic Supplementary Information (ESI) available: [Size, shape and chemical analysis of the nanocones are shown in supplementary information]. See DOI: 10.1039/x0xx00000x
‡ These authors contributed equally to this work.

directly exploit NPG as the substrate for the single molecule detection. [23] In this study, we employed NPG as the template for sharp nano-cone (NC) growth. NPG used in this work was prepared by selective dissolution of silver from 100 nm thick white gold leaves.[20, 21] The fabrication process of NC @NPG films is schematically depicted in Figure 1. First, the hydrophobic NPG film is floated on the plating aquatic solution that contains 1mM Au^{3+} and 2mg/mL sodium dodecyl sulfate (SDS). Then, the NPG film along with the solution container is placed in an airtight box filled with hydrazine gas. [5, 24] Hydrazine gas diffuses into the interfaces between the downside of the NPG film and the plating solution through the open nanopores that do not fill with the solution due to the very small nanopore size and the hydrophobic nature of NPG. The reduction reaction between hydrazine and aqueous chloroaurate ions mainly takes place in the vicinity of each nanopore channel, which results in the formation of single-crystal gold nano-cones that epitaxially grow from the downside of NPG into the solution. This growth manner is very analogous to that of stalactites in nature, which proceeds by interface reactions between solid and liquid and is controlled by the slow diffusion of the reduction gas.

Experimental

Materials and Instrumentations

All chemicals used in this study, including tetrachloroauric acid ($HAuCl_4$), sodium dodecyl sulfate (SDS), polyvinyl pyrrolidone (PVP), lysine, and rhodamine 6G (R6G) are purchased from Sigma-Aldrich. Microstructure characterization was performed by atomic force microscopy (AFM, Veeco CP-50-OL) and scanning electron microscopy (SEM, JIB-4600F). Chemical composition was analyzed by energy-dispersive X-ray spectroscope (EDS) equipped in a transmission electron microscope (TEM, JEM-ARM200F). A micro-Raman spectrometer (Renishaw InVia RM 1000) was used for regular SERS measurements. The Raman mappings for the single molecule detection were recorded by using a Nanophoton laser Raman microscope (RAMAN-11) (100×, NA = 0.9). RAMAN-11 features a single-transverse-mode laser to realize spatial resolution better than 500 nm. Ultrafast and stable Raman imaging in line optical scanning mode enables catching hot spots in probed regions, which are highly sensitive and easily missed. The dispersion of the electromagnetic field around NCs was calculated with the discrete dipole approximation (DDA).

Fabrication of NPG

NPG films were prepared by selective dissolution of silver from 100 nm thick white gold leaves (Ag:Au=65:35 at. %) in 71% nitric acid for 6 hours at room temperature. The as-dealloyed NPG films with an average pore size of 30~40 nm were carefully washed with distilled water (18.2MΩ·cm) to remove residual chemicals.

SERS Measurement

SERS spectra were collected using a Renishaw inVia micro-Raman spectrometer with 633 nm(wet samples)/514 nm(dry samples) excitations, and the laser power was set at a low value to avoid possible damage of the probe molecule. SERS mapping image was measured using a Nanophoton laser Raman microscope with 532 nm excitation. The laser power was set at as low as ~0.1 mW to avoid possible damage from laser irritation. In order to calculate the EF, the substrates were sealed up in a capillary tube together with a 10^{-6}M R6G methanol solution. For the incident angle dependent SERS measurements, the NC @NPG substrate was immersed in 10^{-6}M R6G methanol solution for about 30 minutes and then taken out washed with ethanol. After drying in the air the substrate was fixed on a rotatable sample stage for the SERS measurement. The excitation wavelength is 633 nm. The laser power was set at a low value to avoid possible damage of the probe molecule. The accumulation time for the SERS measurement is 50 seconds. All the spectra are the average of the spectra obtained at 10 different sites on the substrates.

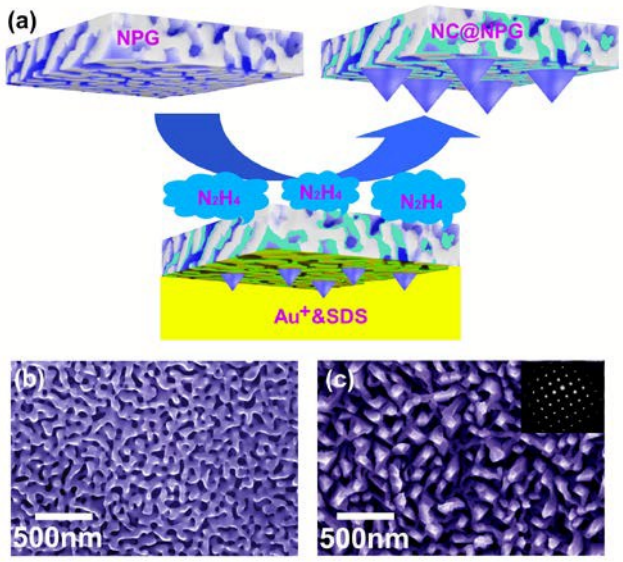

Figure. 1. (a) Schematic diagram of the nano-cones formation at the interface between NPG film and plating solution. (b) SEM micrographs of the as-prepared NPG. (c) SEM image of the nano-cones decorated NPG. The inset shows selected area electron diffraction pattern from the NC@NPG, demonstrating the single-crystal nature of the sample and the epitaxial growth of NC on the NPG substrate.

Results and discussion

We systematically investigated the effects of reactants on the NTs growth and found that the surfactant, sodium dodecyl sulfate (SDS), and the concentrations of Au^{3+} are the key factors controlling the formation of NC. As shown in Figure 2a with a high concentration of 5mM Au^{3+} and 2mg/mL SDS, the growing rate of the NC is very fast and large NC with a random orientation and a low areal density are formed on the NPG film at a short deposition time of 30 minutes. When we reduced the Au^{3+} concentration to 1mM, uniform NC with an orientation perpendicular to the NPG film can be formed with a controllable growth rate (Figure 2b). It was also found that the addition of SDS plays a crucial role in the formation of gold

NC. Without SDS, the gold plating leads to the homogeneous growth of gold ligaments of NPG and NC cannot be formed on the NPG substrates. [5] We also tried other additions, such as lysine (Figure 2c) and Polyvinyl Pyrrolidone (Figure 2d). However, they result in the formation of gold nanoparticles on the NPG film, but not NC. SDS is a common anionic surfactant with one hydrophilic end and one hydrophobic end. Below a critical micellar concentration (~2.4mg/mL), the surfactant molecule adsorption is governed by monomer adsorption. [25-27] SDS molecules may selectively adsorb on specific surfaces of gold ligaments, such as terraces, edges and corners that have a high chemical activity, [28] and leads to the nucleation and growth of plated gold along a preferential direction for the formation of NC by suppressing the uniform growth of gold ligaments. In this study, the optimal plating solution for the controlled NC growth is found to be composed of 1mM Au^{3+} and 2mg/mL SDS.

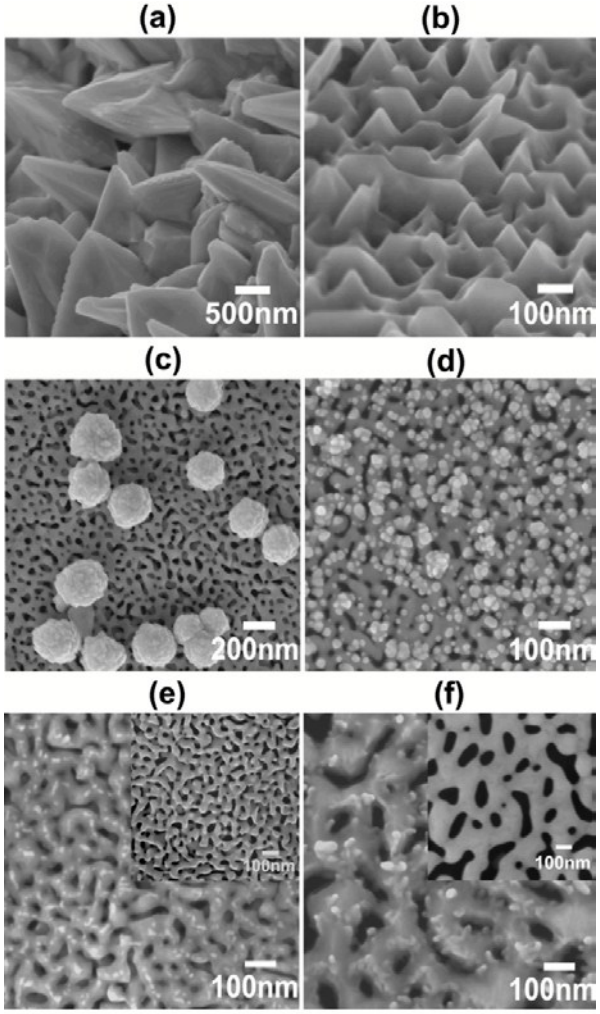

Figure. 2. SEM images of gold-plated NPG prepared with different conditions. (a) The plating solution contains 5 mM Au^{3+} and 2 mg/mL SDS; (b) the solution contains 1 mM Au^{3+} and 2 mg/mL SDS; (c) the solution contains 1 mM Au^{3+} and 2 mg/mL lysine; (d) the solution contains 1 mM Au^{3+} and 2 mg/mL PVP; (e) the as-dealloyed NPG film is used as the substrate; and (f) the annealed NPG film is used as the substrate. The insets shown in (e) and (f) represent the SEM micrographs of the NPG films before gold plating.

With the optimal plating solution, we investigated the influence of nanopore sizes of NPG on the NC growth by annealing the NPG at high temperaturs. For the as-dealloyed NPG substrate, a high density of NC can be observed after 30 minute plating (Figure 2e). After annealing the NPG film at 200°C for 120 minutes, the nanpore size increases from ~30-40 nm to ~90 nm. With the same plating conditions, it can be seen that heterogeneous gold nanoparticles appear on the ligament surface, instead of a high density of NC. Since the terraces and edges and corners of gold ligaments act as the preferential nucleation sites for the plated gold, the small gold ligaments of the as-prepared NPG have more nucleation sites than those in the annealed NPG in which the ligaments become large and the surface turn into smooth because of the surface diffusion and relaxation. [28] The less nucleation sites as well as fast diffusion of the reduction gas through the large pore channels may be the reasons for the formation of heterogeneous nanoparticles on the annealed NPG substrate. Since smaller ligament sizes can provide more nucleation sites for a higher density of NC, we also investigated the NPG with a small pore size of ~10-15 nm. Although small ligaments of the fine NPG film can improve the density of NC, the small pore channels are quickly sealed by the plating gold, which prevents the NC growth. Thus, in this study, the optimal substrate for the NC growth is the as-dealloyed NPG with a 30-40nm ligament and nanopore sizes.

Figure 3a and b are the scanning electron microscope (SEM) and atomic force microscope (AFM) images of the as-dealloyed NPG film. Both ligaments and nanopore channels have a nearly identical diameter of ~30~40nm with a quasi-periodic distribution. Facets and nano-scale embossments can be observed on the gold ligament surfaces, which may act as the preferential sites for the NC nucleation and growth. Figure 3c and d show the stereoscopic images of NC with the plating time of 90 minutes and 180 minutes, respectively. For both samples, NC uniformly distribute on the surfaces of the NPG substrates. With 90 minutes plating the NC (NC1@NPG) have an average length of ~40 nm with an apex of ~10-20 nm (Figure 3c). The density of NC is measured to be 40-46 μm^{-2}, which is higher than or at least comparable to those of the nano-patterns fabricated by the lithography and focus ion beam. [4] Further increasing the plating time to 180 minutes, the average length of the NC (NC2@NPG) grows to ~80 nm but the tip apex remains as ~10-20 nm (Figure 3d). Although individual NC in each sample looks slightly different in sizes, they are very similar to each other in the shape and have a nearly constant length to width ratio and a sharp tip apex (*see* **Figure S1** in the Supplementary Information). Separate TEM characterization reveals that the NC have a face-centered cubic (f.c.c.) structure whereas obvious interfaces between the NC and NPG substrates cannot be found, further confirming the epitaxial growth mechanisms of NC (Figure 1c). Moreover, chemical analysis indicates the composition of the NC is pure gold (*see* **Figure S2** in the Supplementary Information). The density and size of NC can be well controlled by the deposition time (*see* **Figure S3** in the Supplementary Information) and, in

general, shorter deposition time gives rise to a higher density of NC with a shorter length.

The distribution of electric field around the apex of a NC is verified by a near-field Disctete-dipole approximation (DDA) calculation [29] in which a simplified nanostructure with a conical profile representing the key structural feature of individual NC is introduced to qualitatively simulate the optical properties (**Figure 4a**). The nanostructure used in the simulation has the same length to width ratio determined by experimental measurements and a spherical apex with a diameter of 10 nm. Under the plane wave with wavelength of 633 nm propagating along the direction that is intersected with perpendicular bisector of the cone by θ=45°, the near-field ($|E|^2$) distributions are presented in **Figure 4b**. A large enhancement of the electric field at the apex of the NC can be observed and the local electromagnetic enhancement factor is approximately 10^5 by comparing the local maximum intensity with that of the incident light. Also, the coupling effect between adjacent NC and neighboring ligaments, [23] which haven't been taken into the simulation, might further enhance the electric field intensity. Moreover, the apexes of NC bear highly curved features, and these regions have more coordinatively unsaturated atoms that can affect their chemical reactivity and surface bonding properties and act as preferred binding sites for analyte molecules. Thus, the curved region at the apex is expected to provide an improved chemical effect with additional two or three orders of magnitudes enhancement. [30]

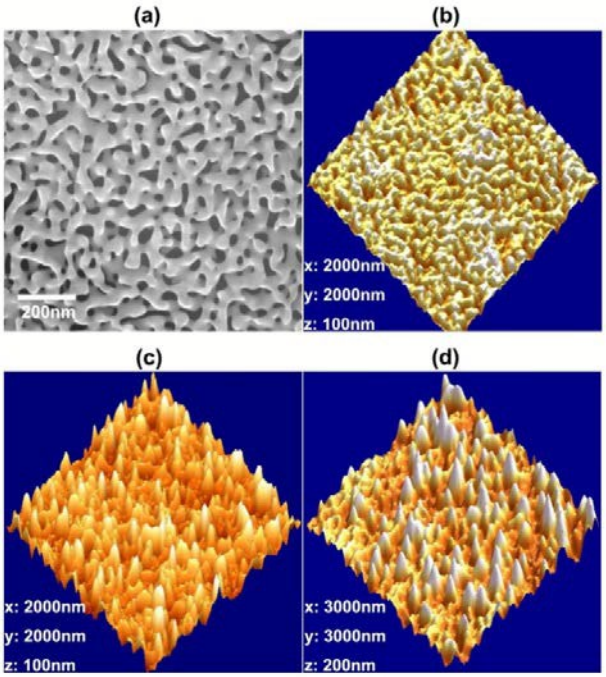

Figure. 3. Microstructure of as-dealloyed NPG and NC@NPG. (a)SEM micrograph of the as-prepared NPG; (b) AFM image of as-prepared NPG with a ligament size of 30~40 nm; (c)Stereoscopic AFM image of nano-cones on the NPG surface with the plating time of 90 minutes; and (d) AFM image of nano-cones on the NPG surface with the plating time of 180 minutes.

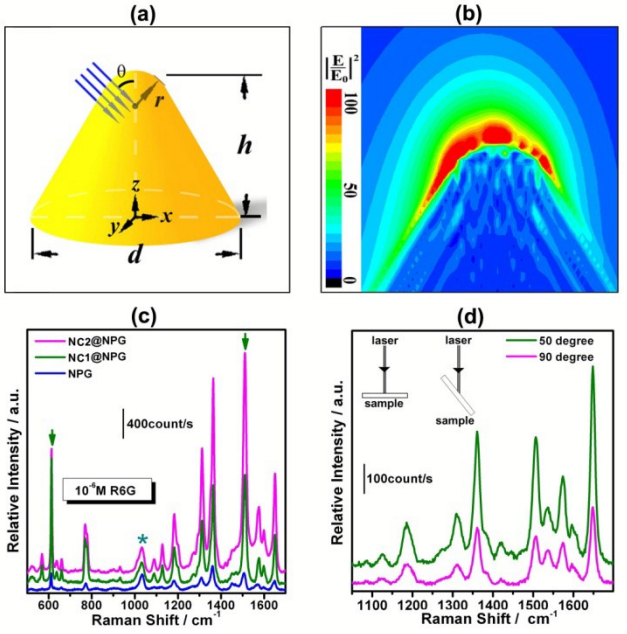

Figure. 4. Electric field distribution of a nano-cone and SERS performance of NC@NPG. (a) A simplified model of a gold nano-cone for the simulation of the interaction between nano-cone and incident light, d=80 nm, h=40 nm, r=10 nm and θ=45°; (b) focused electric field at the apex of the nano-cone; (c) SERS spectra of 10^{-6}M R6G methanol solution from NPG and NC2@NPG with 633 nm excitation at the laser power of 3 mW; and (d) SERS spectra of R6G on NC2@NPG with different incident angles (633 nm excitation, and the laser power of at the sample is about 0.06 mW). The intensity of the electric field is normalized with the energy of incident light (E_0), i.e $|E/E_0|^2$.

The dye molecule rhodamine 6G (R6G) in methanol is used to characterize the SERS enhancement of NC@NPG. (The details of the SERS experiment are introduced in the Experimental Methods.) The SERS spectra of R6G are shown in **Figure 4c**, in which the strongest band at 613 cm^{-1} is assigned as an in-plane bending of the xanthene ring. [31] High-frequency bands at 1312, 1363, and 1511 cm^{-1} with large scattering cross-sections are assigned to the stretching modes of aromatic benzene rings. It is worth noting that the NC@NPG substrate shows a dramatically improved SERS enhancement compared to the as-prepared NPG. The Raman intensity of 1539 cm^{-1} band is over 20-fold for NC2@NPG and over 10-fold for NC1@NPG higher than that from the as-prepared NPG. The differential Raman cross section of R6G excited at 633 nm ($\sigma_{R6G,\ SERS}$) compared to that of methanol (σ_{meth}) can be estimated by the follow quation: [32, 33]

$$\sigma_{R6G,\ SERS}/\sigma_{meth} = [I_{R6G}/C_{R6G}] / [I_{meth}/C_{meth}], \quad (1)$$

where the I_{R6G} and I_{meth} are the intensity of the chosen vibrational modes of R6G (marked with arrows) and methanol (marked with star) in **Figure 4c**, respectively. C_{R6G} and C_{meth} are the concentrations of R6G and methanol. The Raman cross section of R6G is determined by comparing the integrated areas of the R6G bands with the methanol C-O stretch band at ~1030 cm^{-1}. [34] According to Eq.1, the calculated Raman cross

sections ($\sigma_{R6G, SERS}$) of 613 cm^{-1} and 1511 cm^{-1} bands of R6G are 6×10^{-21} cm^2/molecule and $5\times10^{-20}cm^2$ /molecule, respectively. Compared with the normal Raman cross section ($\sigma_{R6G, NR}$) of the two bands (*see* **Figure S4** in the Supplementary Information), [32] the enhancement factor (EF) can be estimated by:

$$EF = \sigma_{R6G, SERS} / \sigma_{R6G, NR} \quad (2)$$

The average EF of NC2@NPG is ~10^7. Since the SERS intensity is dominantly from a small fraction of molecules adsorbing at the electromagnetic "hot spots" [35-38] and the effective area fraction of nano-cones in the detected region is smaller than 1%, the EF of individual nano-cones is estimated to be ~10^8-10^{10}. Moreover, consistent with the DDA simulation, the SERS enhancement of NC@NPG strongly depends on the incident angle of the laser beam. When the sample is tilted to 40-50° with respect to the laser beam, the enhancement can be further improved to four times stronger than that obtained with a 90° angle as shown in **Figure 4d**.

The high EF of NC@NPG film implies possible single molecule detection from the NTs with a sharp apex. Figure 5 shows the Raman mappings of the specimen with different coverage of R6G molecules. The average surface density of the probe molecules is ~25 per μm^2 of the geometric area of the surface for the 1×10^{-10} M solutions (**Figure 5a** and **b**). The molecule coverage decreases to ~0.25 per μm^2 (**Figure 5c** and **d**) when a 1.0×10^{-12} M solution is used. [38] The hot spots with the strong SERS signals are originating from the apex of the NC, which are determined by Raman fingerprints from individual bright dots in the Raman mappings. The number density of the hot spots is ~1.6/μm^2 for 10^{-10} M R6G. **Figure 5b** are example of the Raman spectra from the hot spots. All the Raman bands of R6G can be observed, showing the ensemble spectral characteristics from multiple molecules. Moreover, the detectable spectral variation in the band intensity and width indicates that the recorded Raman signals from individual hot spots originate from a small number of molecules. When the molecule coverage is further decreased to less than 1 molecule per μm^2 by using the 1.0×10^{-12} M solution (**Figure 5c**), the density of the hot spots decreases to 0.01/μm^2. It can be seen that the spectral difference becomes apparent due to the loss of the ensemble averaging and indicates that the SERS detection of individual NC reaches thesingle molecule regime. Strong spot-to-spot variation can be observed for all band parameters, including Raman shift, bandwidth, band shape, and absolute and relative intensity (**Figure 5d)**, which is associated with the dynamics and unique environment of the single molecule as well as the electromagnetic field variation at each hot spot. Moreover, the adsorption status of each molecule at the hot spots depends on several experimental variables including molecular orientation, surface charge and adsorption kinetics, which also gives rise to the unique single-molecule Raman spectra.

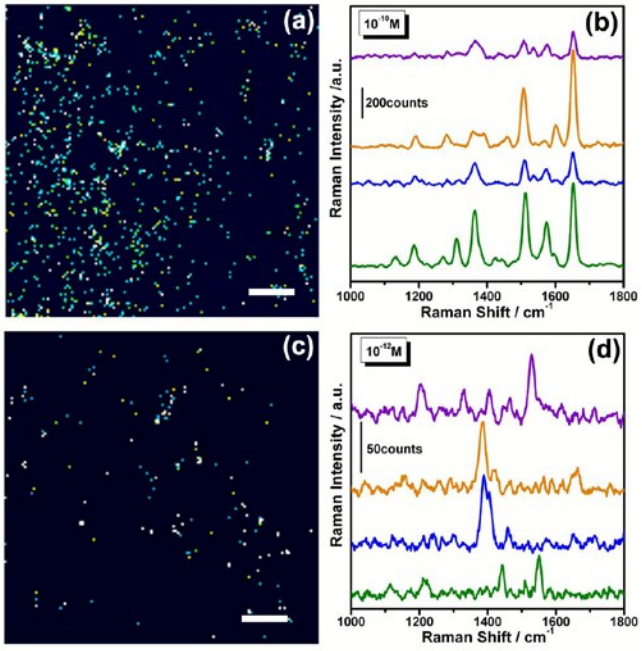

Figure. 5. SERS intensity mappings and spectra of R6G on NC2@NPG showing the single molecule detection. (a) SERS mapping of 10^{-10} M R6G; and (b) four selective SERS spectra recorded from different hot spots. (c) SERS mapping of 10^{-12} M R6G; and (d) four selective SERS spectra recorded from different hot spots. Mappings are based on the characteristic band of R6G range from 600 cm^{-1} to 1800 cm^{-1}. The scale bars in the maps are 5 μm.

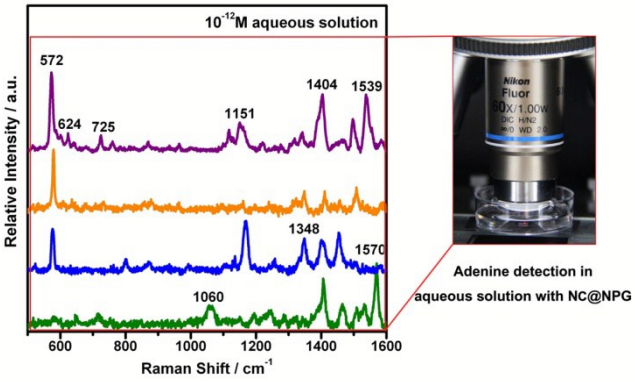

Figure. 6. Single molecule detection in aquesous solution with NC2@NPG. The left shows four selective SERS spectra recorded from different hot spots on NC2@NPG in 10^{-12}M adenine aqueous solution, and the right shows the experiment photo set-up for the SERS measurement.

To further confirm the suitability of the NC@NPG for single molecule SERS detection, we investigated an optically nonresonant bio-molecule (e.g. adenine) with point laser excitation (Renishaw InVia RM 1000, 633nm). Figure 6 shows the SERS spectra of adenine from 10^{-12}M aqueous solution. The assignments of the characteristic peaks are listed in Supplementary Information (Table S1). Considered the detective volume as a cylinder with the 15μm^2 bottom area and 110μm hight, the estimated detective molecule is less than one. Moreover, spot-to-spot variation also can be observed for all band parameters, which further evidences single adenine molecule detection in aqueous solution.

Conclusions

We have developed a facile method to fabricate the high density and large scale of NC by utilizing the open nanopore channels of free-standing NPG films. High SERS enhancements can be achieved at the apexes of the NC for the single-molecule detection. The biocompatible and free-standing NC@NPG films with a high density of electromagnetic hot spots hold unique promise for the applications in ultrasensitive instrumentation for molecular diagnostics and single-molecule analysis.

Acknowledgements

This research was sponsored by JST-CREST "Phase Interface Science for Highly Efficient Energy Utilization"; and "World Premier International Research Center (WPI) Initiative" MEXT, Japan.

Notes and references

1 K. Hering, D. Cialla, K. Ackermann, T. Dörfer, R. Möller, H. Schneidwind, R. Mattheis, W. Fritzsche, P. Rösch, J. Popp, *Anal. Bioanal. Chem.* 2008. **390**, 113-124.
2 N. P. W. Pieczonka, R. F. Aroca, *Chem. Soc. Rev.* 2008, **37**, 946-954.
3 J. M. Banholzer, E. J. Millstone, L. Qin, A. C.Mirkin, *Chem. Soc. Rev.* 2008, **37**, 885-897.
4 D. E. Diebold, P. Peng, E. Mazur, *J. Am. Chem. Soc.* 2009, **131**, 16356-16357.
5 X. Y. Lang, L. Y. Chen, P. F. Guan, T. Fujita, M. W. Chen, *Appl. Phys. Lett.* 2009, **94**, 213109.
6 S. J. Biteen, D. Pacifici, S. N. Lewis, A. Atwater, H. *Nano Lett.* 2005, **5**, 1768-1773.
7 D. Graham, G. D.Thompson, E. W. Smith, K. Faulds, *Nat. nano technol.* 2008, **3**, 548-551.
8 D-K. Lim, K-S. Jeon, M. H. Kim, J-M. Nam, D.Y. Suh, *Nat. Mater.* 2010, **9**, 60-67.
9 L. Zhang, X. Y. Lang, A. Hirata, M. W. Chen, *ACS Nano.* 2011, **5**, 4407-4413.
10 J. M. Banholzer, D. K. Osberg, S. Li, F. B. Mangelson, C. G. Schatz, A. C. Mirkin, *ACS Nano.* 2010, **4**, 5446–5452.
11 J. Xie, Q. Zhang, Y. J. Lee, I. C. D. Wang, *ACS Nano.* 2008, **2**, 2473-2480.
12 P. F. Liao, A. Wokaun, *J. Chem. Phys.* 1982, **76**, 751-752.
13 J. C.Hulteen, R. P. Van Duyne, *J. Vac. Sci. Technol. A* 1995, **13**(3), 1553-1558.
14 D. Cialla, U. Hubner, H. Schneidewind, R. Moller, J. Popp. *Chem. Phys. Chem*. 2008, **9**, 758-762.
15 P. J. Schuck, D. P. Fromm, A. Sundaramurthy, G. S. Kino, W. E. Moerner, *Phys. Rev. Lett.* 2005, **94**, 017402.
16 N. C. Linn, C. H. Sun, A. Arya, B. Jiang, P. Jiang, *Nanotechnology* 2009, **20**, 225303.
17 V. Guieu, D. Talaga, L. Servant, N. Sojic, F. Lagugné-Labarthet, *J. Phys. Chem. C* 2009, **113**, 874-881.
18 Y. Yang, M. Tanemura, Z. Huang, D. Jiang, Z. Li, Y. Huang, G. Kawamura, K. Yamaguchi, M. Nogami, *Nanotechnology* 2010, **21**,325701.
19 Y. Sawai, B. Takimoto, H. Nabika, K. Ajito, K Murakoshi, *J. Am. Chem. Soc.* 2007, **129**, 1658-1662.
20 L. H. Qian, X. Q. Yan, T. Fujita, A. Inoue, M. W. Chen, *Appl. Phys. Lett.* 2007, **90**, 153120.
21 Y. Ding, Y. Kim, J. Erlebacher, *Adv. Mater.* 2004, **16**, 1897-1900.
22 T. Fujita, L. H. Qian, K. Inoke, J. Erlebacher, M. W. Chen, *Appl. Phys. Lett.* 2008, **92**, 251902.
23 X. Y. Lang, P. F. Guan, L. Zhang, T. Fujita, M. W. Chen, *J. Phys. Chem. C* 2009, **113**, 10956–10961.
24 Y. Ding, J. Erlebacher, *J. Am. Chem. Soc.* 2003, **125**, 7772-7773.
25 J. P.Deng, C. Wu, C. H. Yang, C. Y. Mou, *Langmuir* 2005, **21**, 8947-8951.
26 A. A. Levchenko, B. P. Argo, R. Vidu, R. V. Talroze, *Langmuir* 2002, **18**, 8464-8471.
27 C. H. Kuo, T. F. Chiang, L. J. Chen, M. H. Huang,. *Langmuir* 2004, **20**, 7820-7824.
28 T. Fujita, P. Guan, K. McKeena, X. Y. Lang, A. Hirata, L. Zhang, T. Tokunaga, S. Arai, Y. Yamamoto, N. Tanaka, Y. Ishikawa, N. Asao, Y. Yamamoto, J. Erlebacher, M. W. Chen, *Nat. Mater.* 2012, **11**, 775-780.
29 T. B. Draine, J. P. Flatau, *J. Opt. Soc. Am. A* 1994, **11**, 1491-1499.
30 M. Moskovits, *Rev. Mod. Phys.* 1985, **57**, 783-826.
31 H. Watanabe, N. Hayazawa, Y. Inouye, S. Kawata, *J. Phys. Chem. B* 2005, **109**, 5012-5020.
32 S. H. Ciou, Y. W. Cao, H. C. Huang, D. Y. Su, C. L. Huang, *J. Phys. Chem. C* 2009, **113**, 9520-9525.
33 A. Kudelski, *Chem. Phys. Lett.* 2005, **414**, 271-275.
34 S. Shim, M. C. Stuart, A. R. Mathies, *Chem. Phys. Chem.* 2008, **9**, 697-699.
35 Y. Fang, N-H. Seong, D. D. Dlott, *Science* 2008, **321**, 388-392.
36 M. S. Wells, D. S. Retterer, M. J. Oran, J. M. Sepaniak, *ACS Nano.* 2009, **3**, 2845-2853.
37 M. Hu, S. F. Ou, W. Wu, I. Naumov, X. Li, M. A. Bratkovsky, R. S. Williams, Z. Li, *J. Am. Chem. Soc.* 2010, **132**, 12820–12822.
38 H. W. Liu, L. Zhang, X. Y. Lang, Y. Yamaguchi, H. Iwasaki, Y. Inouye, Q. K. Xue, M. W. Chen, *Scientific Reports.* 2011, **1**, 112-116.

Quasi-periodic nano-cone arrays uniformly sprout on the centimeter-sized free-standing nanoporous gold (NPG) films *via* Au plating, and the nano-cones@NPG serve as a high-performance SERS substrate.